Scientific Reports

https://doi.org/10.1038/s41598-026-45009-y

Article in Press

An enhanced novel surface plasmon resonance sensor employing perovskite nanomaterial and bismuth ferrite to identify different ethanol concentrations

Received: 4 December 2025

Accepted: 16 March 2026

Published online: 02 May 2026

Cite this article as: Daher M.G., Abukhadra M.R., Srour S.M. *et al.* An enhanced novel surface plasmon resonance sensor employing perovskite nanomaterial and bismuth ferrite to identify different ethanol concentrations. *Sci Rep* (2026). https://doi.org/10.1038/s41598-026-45009-y

Malek G. Daher, Mostafa R. Abukhadra, Samer M. Srour, Emad Solouma, Stefano Bellucci, Haifa A. Alqhtani, Hussein A. Elsayed & Ahmed Mehaney

An enhanced novel surface plasmon resonance sensor employing perovskite nanomaterial and bismuth ferrite to identify different ethanol concentrations

Malek G. Daher[1,2*], Mostafa R. Abukhadra[3,*], Samer M. Srour[1], Emad Solouma[4], Stefano Bellucci[5], Haifa A. Alqhtani[6], Hussein A. Elsayed[7], and Ahmed Mehaney[7]

[1]Physics Department, Islamic University of Gaza, P.O. Box 108, Gaza, Palestine
***Corresponding Author E-mail:** malekjbreel20132017@gmail.com
Email: samermoeen.2001@gmail.com
[2]Information Technology Faculty, University College of Applied Sciences, Gaza, Palestine

[3]Geosciences Department, College of Science, United Arab Emirates University, 15551, Al Ain, United Arab Emirates
(m.abdelwahab@uaeu.ac.ae)

[4]Department of Mathematics and Statistics, College of Science, Imam Mohammad Ibn Saud Islamic University (IMSIU), Riyadh, 11623, Saudi Arabia (emmahmmsoud@imamu.edu.sa)
[5] INFN-Laboratori Nazionali di Frascati, Vie. E. Fermi 54, 00044 Frascati, Italy (bellucci@inf.infn.it)
[6]Department of Biology, college of Science, Princess Nourah bint Abdulrahman University, P.O. BOX 84428, Riyadh 11671, Saudi Arabia (haifaAlqhatani@bnu.edu.sa)
[7]Photonic and phononic crystals Lab., Physics Department, Faculty of Science, Beni-Suef University, Beni-Suef, 62512, Egypt (ahmed011236@science.bsu.edu.eg , drhussien85sc@gmail.com)

Corresponding Author: Malek G. Daher (malekjbreel20132017@gmail.com, m.abdelwahab@uaeu.ac.ae)

Abstract

This study presents a novel surface plasmon resonance (SPR) biosensor composed of silver (Ag), bismuth ferrite (BiFeO3), nickel (Ni), and perovskite nanomaterial (MAPbBr3). Different ethanol concentrations (ECs) could be detected thanks to the hybrid structure. The transfer matrix technique (TMM) is used to assess the suggested surface plasmon resonance (SPR) structure. To compare the angular sensitivity of the EC=0% sample with the EC=10% to 40% sample, a comparative analysis was carried out. The BiFeO3, Ni, and MAPbBr3 layer thicknesses must be changed in order to maximize the surface plasmon resonance (SPR) structure's performance. Additionally, precise measurements of the resonance angle (θ_res), minimum reflectance (Rmin), full width at half maximum (FWHM), and figure of merits (FOM) have been made. In comparison to the conventional structure (BK7/Ag/SM) with a matching FOM of 149.12 RIU-1, the ideal angular sensitivity was found to be 55 nm for Ag, 5 nm for BiFeO3, 20 nm for Ni, and 3 nm of MAPbBr3 with a sensitivity of 428 Degree RIU-1, which improved by 268.96%. Furthermore, the impacts of four sensor structures—conventional (BK7/Ag/SM), with BiFeO3 (BK7/Ag/BiFeO3/SM), with Ni (BK7/Ag/BiFeO3/Ni/SM), and our suggested sensor structure (BK7/Ag/BiFeO3/Ni/MAPbBr3/ SM) on sensitivity were examined in this work. The proposed structure shows better angular sensitivity compared to the existing surface plasmon resonance (SPR) biosensor. The biosensor in question shows promise for identifying a broad variety of chemical molecules and biological analytes because of its increased sensitivity.

Keywords

SPR, ethanol, BiFeO3, Sensitivity, biosensor, perovskite.

Introduction

Ethanol is an essential material for biosensing systems that measure the amount of alcohol in food, beverages, and wine. Foods and beverages are preserved for a long time by the addition of ethanol. As a result, identifying excessive ethanol content in meals, beverages, and even medications is crucial. When measured optically, a liquid's refractive index (RI) is affected by the amount of ethanol present. A liquid's RI value is altered in relation to a liquid's RI at zero concentration when the amount of ethanol in the liquid changes. As a result, RI sensing can be useful in determining the amount of ethanol present in different bioliquids. Surface plasmon resonance (SPR)-based biosensors have recently demonstrated impressive uses [1] in organic and biochemical recognition [5], food protection [3], medicinal detection [4], and environmental monitoring [2]. Transverse electromagnetic (TM) waves produced at the border of two substances with conflicting permittivity rates metal (such as Ag, Au, Cu,...) and dielectric cooperate with the free electrons within to materially create surface plasmon (SP) [6,7]. Two-dimensional nano-materials have been crucial in the development of nanophotonic and SPR sensors in recent decades [8,9]. Our goal is to investigate structures for sensitive SPR sensors that be able to identify chemical and organic components with less variation in the sensing medium's RI [5, 10] and that can be experimentally implemented using straightforward manufacturing techniques. We selected the Kretschmann design, which works on the basis of Attenuated Total Reflection (ATR) [11]. In order to augment the performance of these SPR sensors—specifically, the sensitivity of detection—a number of studies on SPR structures have been conducted. SPR structures using an amalgamation of FeO3, Ag, Ni, and

2D nano-materials were proposed recently [12-14]. They got the highest sensitivity as 395 degree/RIU. Here, we propose a hybrid SPR structure comprising Ag formed on a prism of BK7 utilizing nickel (Ni) and bismuth ferrite (BiFeO3) coated by a perovskite material ($MAPbBr_3$) to improve the SPR biosensing performance (see Fig. 1). In our SPR design, Ag is selected as plasmonic material. Ag provides suitable sensitivity, accurate recognition quality with low costs, while having worse chemical stability than other metals like copper and gold [15]. We positioned the Ag metal layer between dielectric materials to improve sensor performance and shield it from oxidation. BiFeO3 is a hopeful material that has drawn interest from investigators because of its tiny optical band gap, increased electric field absorption, and wide range of applications [16–18]. Ni film deposition on Ag/BiFeO3 has two benefits: first, it can shield it from oxidation; second, using a bimetallic amalgamation with Ag raised the efficiency to an extremely high point [12,19]. According to [20], these BiFeO3 and Ni substances produce a superior nanoplasmonic response by penetrating deeply into the sensing medium. Furthermore, we covered the SPR structure with a sheet of organic–inorganic perovskite material, which can be stated as MAPbBr3 with A = NH3 and M = CH3, in order to improve the analytes absorption and create more sensitive SPR sensors. Researchers are becoming more interested in these perovskite materials because they are less expensive, solution-processed nano-materials with potential uses [21]. The sensitivity of MAPbBr3 to heat, oxygen, moisture, and UV radiation causes phase breakdown and disintegration into $PbBr_2$ and volatile components, making it unstable. Encapsulation, surface passivation, compositional engineering (cation/anion mixing), and the use of more resilient inorganic or quasi-2D perovskite structures can increase operational stability. A superior option for SPR biosensor applications, MAPbBr3 is a novel kind of plasmonic nanomaterial [14]. Because of its stronger Pb–Br interactions, $MAPbBr_3$ (methylammonium lead bromide) exhibits more stability than iodide perovskites. It is still susceptible to light, heat, and moisture, though, which can lead to slow deterioration. Its operational stability is greatly increased by appropriate encapsulation and a regulated atmosphere. Because of its tiny band gap, high optical absorption, and outstanding stability, it possesses excellent electrical and optical properties [22, 23]. Presenting an SPR sensor with extremely high efficiency and good resolution in comparison to previous plasmonic designs and the standard SPR structure is the primary driving force behind this work. The optimized biosensor with the perovskite layer (BK7/Ag/BiFeO3/Ni/MAPbBr3/SM) has a sensitivity of 428 deg/RIU, which is 268.96% higher than that of the traditional

SPR sensor. Furthermore, we use the perovskite layer to achieve an excellent FOM of 149.12 RIU−1. These findings are derived using a wavelength excitation at 633 nm and a sensing medium with an ethanol content (EC) of 10%.The novelty of our work is as follow: we have detected ethanol concentrations using SPR structure for the first time. Furthermore, our proposed sensor have attained ultra-high sensitivity which is not in a lot of the similar structures. Finally, the suggested sensor is low cost, label-free detecting, and tiny time spending. With these crucial advantages, it is envisioned that the considered SPR structure can be strongly progressed for ethanol levels detection and bio-medical analyses.

Materials and Methods

Many researchers use the crucial features of Kretschmann's structures in their theoretical model for the development of surface plasmon resonance (SPR) detectors. The SPR method uses the attenuated total reflection methodology to optically induce surface plasmon waves (SPWs). Figure 1 shows the five main layers that make up the suggested biosensor. The operational wavelength is chosen to be 633 nm, which is the wavelength of a light source. The surface plasmon wave's propagation length in SPR sensors is the distance it travels along the metal surface before decaying. The evanescent field's penetration depth is the extent to which it penetrates the detecting medium.

The interaction area and signal stability are impacted by the propagation length.

Surface binding sensitivity and sensing depth are determined by penetration depth.

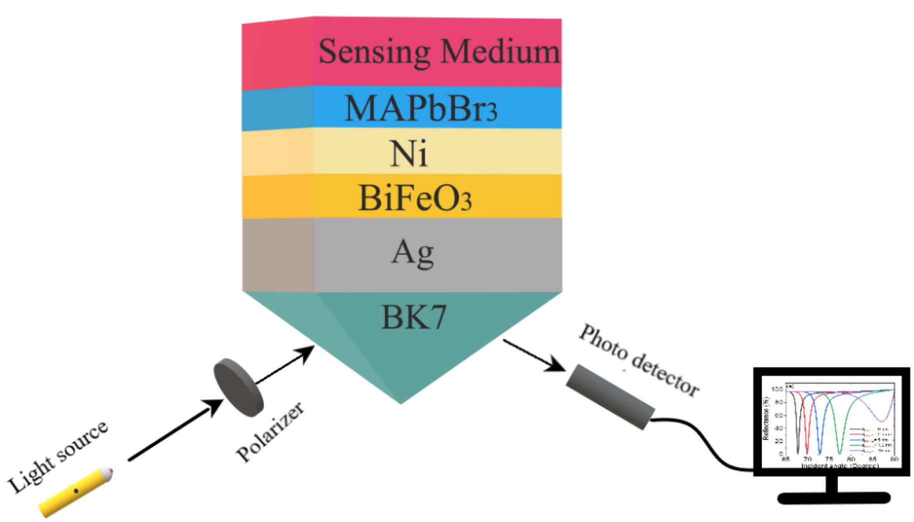

Figure. 1. The projected BK7/Ag/$BiFeO_3$/Ni/$MAPbBr_3$/SM hybrid structure-based SPR biosensor for ethanol concentration (EC) detection.

Mathematical Modeling

The first sheet is built of BK7 prism. This substrate's RI (nBK7 = 1.5151) shifts the reflectance curve in comparison to another prism and significantly increases the biosensor's angular sensitivity. The BK7 prism's refractive index can be calculated as [24] .

$$n_{BK7}(\lambda) = \sqrt{\frac{1.03961212\lambda^2}{\lambda^2 - 0.0060069867} + \frac{0.231792344\lambda^2}{\lambda^2 - 0.0200179144} + \frac{1.01046945\lambda^2}{\lambda^2 - 103.560653} + 1} \quad (1)$$

In order to activate surface plasmon polaritons (SPPs), Ag with a complicated RI of 0.05626+4.2776i and a constant thickness of 55 nm is utilized after the prism [25]. The Drude–Lorentz model can be used to express the refractive index of Ag film [26]:

$$n_{Ag}(\lambda) = \sqrt{1 - \frac{\lambda_c \lambda^2}{\lambda_p^2(\lambda_c + i\lambda)}} \quad (2)$$

where $\lambda_c = 1.7614 \times 10^{-5}$m and $\lambda_p = 1.4541 \times 10^{-7}$m are the collision and plasma wavelengths of Ag. i is the complex number.

Bismuth ferrite (BiFeO3), the third layer, has a refractive index that is highly sensitive to changes in wavelength in the visible spectrum [27]. The refractive index of BiFeO3 for the current study at a wavelength of 633 nm is n□□□□□3 = 2.9680 [28]. The BiFeO3 layer's thickness has been fluctuating between 0 and 10 nm.

A layer of BiFeO3 has been covered with a nickel (Ni) nanofilm. Eq. (2) calculates the refractive index of Ni in the same manner as it does for the Ag metal layer. For Ni, the appropriate collision and plasma wavelengths are □□ = 2.8409 × 10−5 m and 2.5381 × 10−7 m, respectively [20, 29]. Its complex RI at □ = 633 nm is n□□ = 0.031957+2.963i [12].

Furthermore, our suggested nanostructure's fifth layer, MAPbBr3, which is placed between the sensing medium and the Ni metal film, can improve sensor performance. Its complicated RI is n□□□□□□3 = 2.008 + 0.0013i [14,30]. With a 0.5 nm step, the MAPbBr3 layer's thickness (□□□□□□□3) ranges from 0 to 3.5 nm. The sensing medium, which is the final layer, uses EC=0% as the reference material and various ethanol concentrations as analytes.

Table 1 Refractive index and material thickness for the proposed biosensor at 633 nm.

Material layers	Refractive index (RI)	Reference
Prism BK7	1.5151	[31]
Silver (Ag)	0.05626+4.2776i	[26]
Bismuth ferrite ($BiFeO_3$)	2.9680	[28]
Nickel (Ni)	0.031957+2.963i	[12]
Perovskite nanomaterial ($MAPbBr_3$)	2.008 + 0.0013i	[14,30]
Ethanol concentration (EC)	EC (0%) = 1.332 EC (10%) = 1.337 EC (20%) = 1.34 EC (30%) = 1.344 EC (40%) = 1.349	[32]

Using the transfer matrix method (TMM) with help of Maple software, the light reflection of the suggested multi-layer SPR biosensor model was calculated; the wave parameters for the N-layer configuration, which specify the connection among the tangential field components of each sheet from the first sheet (Z = Z1=0) to the last sheet (Z = Z_{N_1}), can be expressed as [33]:

$$\begin{bmatrix} Y_1 \\ D_1 \end{bmatrix} = G \begin{bmatrix} Y_{N-1} \\ D_{N-1} \end{bmatrix} \quad (3)$$

Whereas D1 and DN-1 denote the magnetic field components parallel or tangential to the interface at the same locations, Y1 and YN-1 stand for the electric field components parallel or tangential to the border at the boundaries of the first and last sheets, respectively. The TM of the fused N-layer structure is defined as follows for light with plane polarization [34]:

$$G_{ij} = \left(\prod_{k=2}^{N-1} G_k\right) = \begin{bmatrix} G_{11} & G_{12} \\ G_{21} & G_{22} \end{bmatrix} \quad (4)$$

Where

$$G_K = \begin{bmatrix} \cos(\alpha_k) & -\frac{i\sin(\alpha_k)}{X_k} \\ -iX_k\sin(\alpha_k) & \cos(\alpha_k) \end{bmatrix} \quad (5)$$

The light wave's phase variation as it passes through the jth layer is denoted by α_k.

$$\alpha_k = \frac{2\pi}{\lambda} d_k \sqrt{\varepsilon_k - (n_1 \sin(\theta_1))^2}$$
(6)

where ε_k and d_k are the dielectric permittivity and width of the k_{th} layer. λ, θ_1 and n_1 are the wavelength, the angle of incidence and the RI of prism.

Since the SPR waves cannot be stimulated in a different mode without a material that has both negative permittivity and permeability, we limit the investigation to TM polarization. Regarding transverse magnetic waves (TM)

$$X_k = \frac{\sqrt{\varepsilon_k - (n_1 \sin(\theta_1))^2}}{\varepsilon_k}$$
(7)

Basic mathematical processes, Eq (8) can be used to calculate the reflection coefficient.

$$r_p = \frac{(G_{11} + G_{12} X_N) X_1 - (G_{21} + G_{22} X_N)}{(G_{11} + G_{12} X_N) X_1 + (G_{21} + G_{22} X_N)}$$
(8)

The reflection coefficient is thus represented by r_p , while the characteristic matrices are represented by G_{11}, G_{12}, G_{21}, and G_{22}. The reflectivity Rp of a certain multilayer structure is exactly proportional to the reflection coefficient, as shown in Eq (9). The intensity of reflection is computed as [34]:

$$R_p = |r_p|^2$$
(9)

For optical surface wave patterns, it is frequently referred to as Surface Plasmon Resonance (SPR), and it is mostly impacted by the neighboring dielectric's RI. By tracking the resonant angle, we may identify the environmental dielectric by analyzing the shift in the resonant peak brought about by a change in the environmental dielectric's refractive index. The incidence angle, θ_{res}, can then be written as [35]

$$\theta_{res} = \sin^{-1}\left(\frac{1}{n_{BK7}} \sqrt[5]{\frac{n_{Ag}^2 n_{BiFeO_3}^2 n_{Ni}^2 n_{MAPbBr_3}^2 n_{sm}^2}{n_{Ag}^2 + n_{BiFeO_3}^2 + n_{Ni}^2 + n_{MAPbBr_3}^2 + n_{sm}^2}}\right)$$
(10)

Where n_p, n_{Ag}, n_{BiFeO_3}, n_{Ni}, n_{MAPbBr_3}, and n_{sm} are the refractive indices of the prism, Ag, $BiFeO_3$, Ni, $MAPbBr_3$ and sensing medium, respectively.

Simulation Parameters

Sensitivity and FOM are the two main factors that determine how well SPR-based sensors operate. It is better to maximize all parameters while limiting the full width at half maximum (FWHM) so as to improve the functioning of an SPR biosensor [36]. The effect is used to produce various kinds of sensors, many of which have sensitivity as a defining characteristic.

$$S = \frac{\Delta\theta_{res}}{\Delta n}$$

(11)

where the refractive index and resonant angle variances are denoted by $\Delta\theta_{res}$ and Δn, respectively. This disparity between an analyte and a reference substance is computed.

The breadth of the confinement loss peak is measured by FWHM, which stands for full width at half maximum [37]. A lower FWHM could lead to less spectral noise in the SPR response [38]. The ratio of reflectance sensitivity to full width at half maximum (FWHM) is known as the figure of merit (FOM). The quality element is assessed in RIU^{-1}[39]

$$FOM = \frac{S}{FWHM}$$

(12)

Feasibility and Process of Fabrication

By employing physical vapour deposition (PVD) systems such thermal evaporation, a suitable thickness of silver metal layer can be produced on the base of a BK7 prism. The sol-gel method or the chemical vapour deposition (CVD) technique can be used to create a thin layer of BiFeO3 on the metal surface, followed by a nanofilm of Ni. The MAPbBr3 layer can be placed on top of the framework using CVD techniques. Because of its low operating temperature and excellent fabrication quality, atomic layer deposition (ALD) technology can deposit any nanoscale layer.

Results and discussions

As for the outcome, we have examined and refined the impact of three materials on the traditional structure (BK7/Ag/SM): $BiFeO_3$, Ni, and $MAPbBr_3$. First, we examined the plasmonic response of the three SPR biosensor arrangements: Ag/$BiFeO_3$, Ag/$BiFeO_3$/Ni/$MAPbBr_3$ and Ag/$BiFeO_3$/Ni that were suggested in this work. The impact of these arrangements on the efficiency was then examined and contrasted. For SPR biosensors utilized in the biofield, the outcomes of these designs are really encouraging.

Thicknesses optimization of $BiFeO_3$

First, we investigate the impact of the $BiFeO_3$ layer thickness in order to adjust the scheme of the suggested structure. Ag's thickness of 55 nm is maintained under observation. The ideal thickness is one that achieves a reflection dip (R□□□) that goes to zero, boosts the FOM, focusses the intensity of radiation to the detecting surface, and improves sensitivity. The impact of varying $BiFeO_3$ layer thicknesses (d_{BiFeO3} = 0 to 10 nm) is depicted in Figures 2 and 3. For varying BiFeO3 thicknesses (d_{BiFeO3}), Figure 2(a) and (b) illustrate how the reflection changes with the angle of incidence. Figure 2(a) and Figure 2(b) display the curves for two ethanol concentrations in the detection medium: 0% and 10%, respectively. The evolution of the SPR resonance's incidence angle with respect to BiFeO3 thickness is depicted in Figure 3(a). The graphic illustrates how the incidence angle rises as BiFeO3 thickness increases. The sensitivity is best (228 degree/RIU) at a thickness of BiFeO3 of 7.5 nm with FOM = 93.06 1/RIU. The FOM decreased by 38.22% and the sensitivity was enhanced by 96.55% in comparison to the traditional structure (BK7/Ag/SM). The progression of FWHM and FOM against dBiFeO3 is depicted in Figure 3(b). We find that FOM drops nearly linearly with dBiFeO3, reaching 93.06 RIU−1 at dBiFeO3 = 7.5 nm before experiencing a sharp decline at dBiFeO3 = 10 nm. In addition to improved sensitivity, the minimum reflectance need be saved at zero for the best biosensor design. The minimum reflectance Rmin against dBiFeO3 is drawn in Figure 3(c). At dBiFeO3 = 5 nm (corresponding to Rmin = 0.001%), we observe that the reflectance is at its lowest, corresponding to sensitivity and FOM values of 160 deg/RIU and 104.57 RIU−1, respectively. The sensitivity boost of these BiFeO3 is shown as a function of thickness in Figure 3(d). This enhancement is more considerable than that of the conventional sensor and includes 96.55% at dBiFeO3 = 7.5nm. In addition to protecting Ag film from oxidation, BiFeO3 is a suitable nanomaterial that can enhance SPR biosensor performance. It does have several drawbacks, though, like ineffective charge transfer and analyte adsorption rates. The Ni deposition on the BiFeO3 sheet is one way to solve this issue. A bilayer of BiFeO3/Ni that steadies the SPR structure and lowers its production cost is made possible by nickel's exceptional magneto-optical qualities and reduced optical losses [17, 40]. It should be noted that in order to guarantee stable SPR biosensor performance, S. Singh et al. employed an analogous construction with Fe2O3/Ni as protective layers [12].

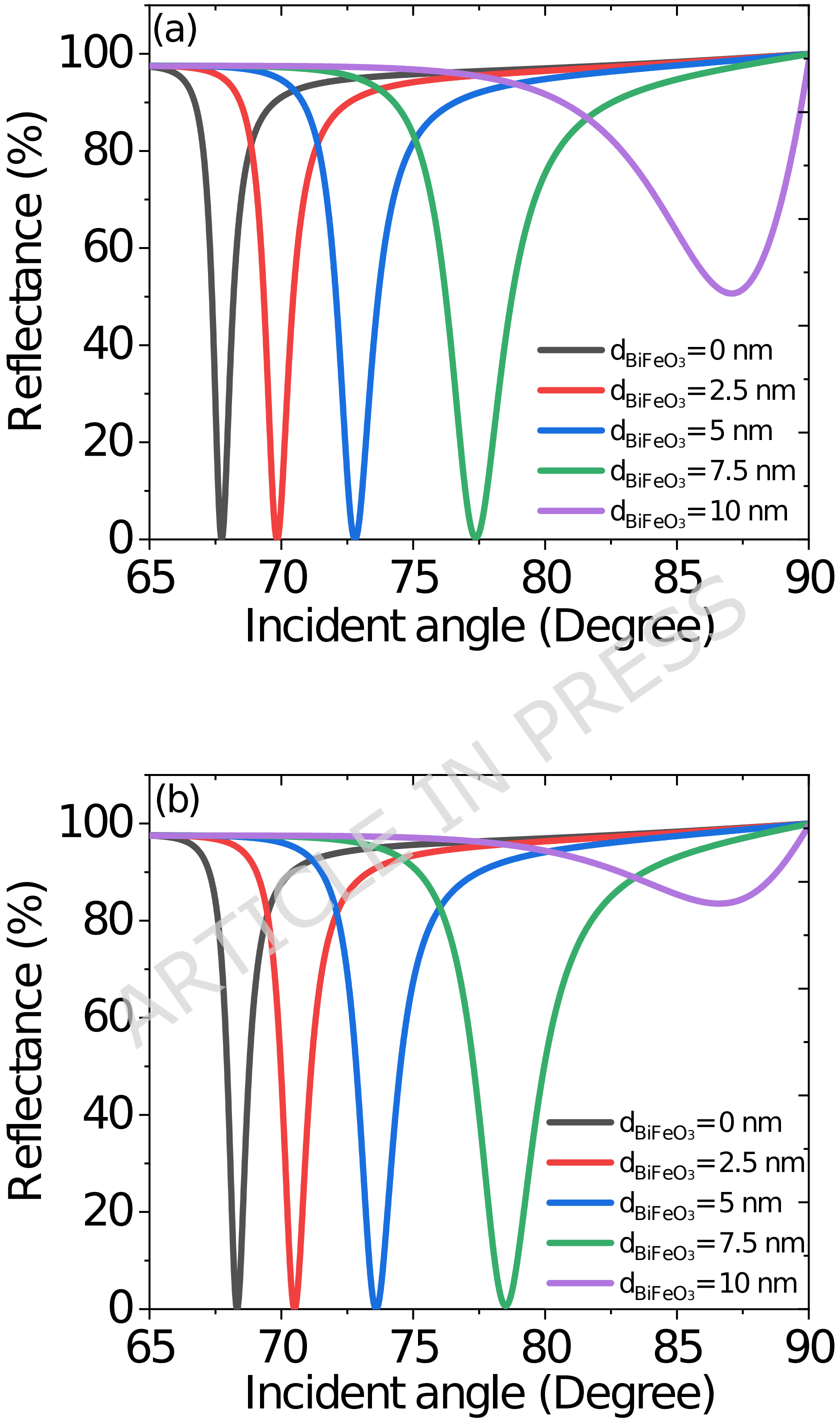

Figure. 2. (a) and (b) Reflectance spectrum for various thickness of $BiFeO_3$ (a) for EC = 0%, (b) for EC = 10%].

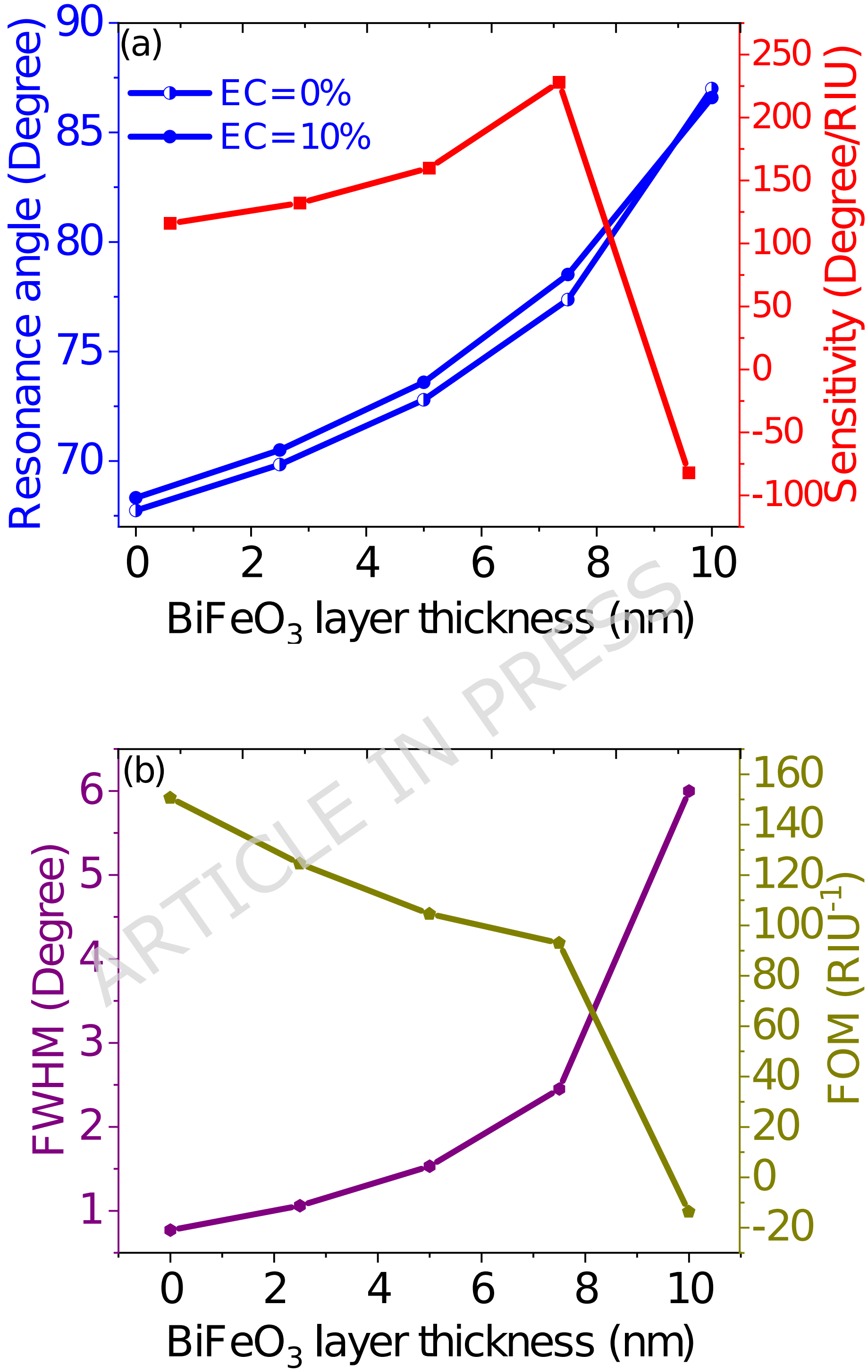

(a)
EC=0%
EC=10%
Resonance angle (Degree)
Sensitivity (Degree/RIU)
90
85
80
75
70
250
200
150
100
50
0
-50
-100
0
2
4
6
8
10
BiFeO3 layer thickness (nm)
(b)
FWHM (Degree)
FOM (RIU-1)
6
5
4
3
2
1
160
140
120
100
80
60
40
20
0
-20
0
2
4
6
8
10
BiFeO3 layer thickness (nm)

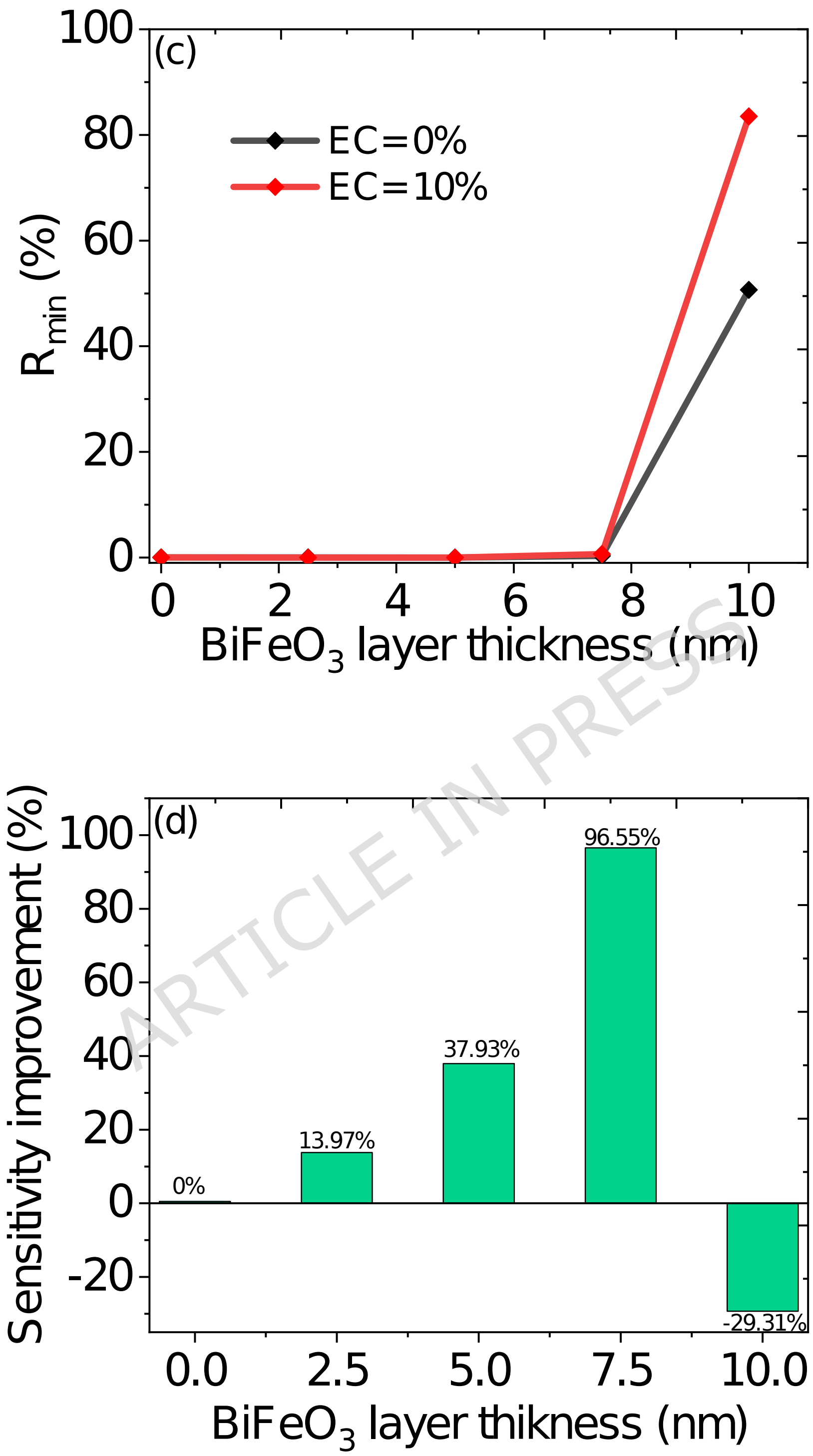

Figure. 3. (a) Development of the sensitivity of SPR structure with thickness of $BiFeO_3$, (b) FWHM and FOM alternative with $BiFeO_3$ thickness for projected structure of BK7/Ag/$BiFeO_3$, (d) Minimum reflectance (R_{min}) values with $BiFeO_3$ thickness for various analyte refractive index and (c) Sensitivity

enhancement as a function of the $BiFeO_3$ layer thickness for proposed SPR biosensor.

Impact of Ni layer deposition

We investigate how the suggested structure is affected by Ni thickness. Five nanometers is the fixed thickness of BiFeO3. The reflectance vs the incident angle for various Ni nanofilm thicknesses (d□□ = 0 to 30 nm) is displayed in Figure 4. It should be noted that the dips moves to upper angles of incidence as the Ni thickness increases. The ethanol concentration (EC) (EC = 0% in Figure 4(a) and EC = 10% in Figure 4(b)) has no bearing on this characteristic. Let's also observe that as the Ni thickness increases, the resonant dip's quality factor rises. The development of sensitivity, FOM, and FWHM against d□□ will be examined in the sections that follow. The development of the angle of resonant dip against d□□ for two values of the detecting medium's EC is displayed in Figure 5(a). We plotted the sensitivity against d□□ in the same figure. We observe that for d□□ = 30 nm with Rmin = 60.54%, the sensitivity rises with Ni width to touch 272 deg/RIU, indicating a weak optical response that is unsuitable for an SPR biosensor for d□□ > 20 nm. The development of FOM and FWHM against d□□ is depicted in Figure 5(b). In order to obtain 188.88 RIU−1 at d□□ = 30 nm, we find that FOM increases roughly linearly with d□□. It should be noted that the FOM is improved by 25.38% when contrasted to the traditional structure and by 80.62% when contrasted to the BK7/Ag/BiFeO3 structure when the Ni sheet with d□□ = 30 nm is added to the nanostructure. The sensitivity augmentation against Ni layer thickness is displayed in Fig. 5(c); at d□□ = 30, this enhancement is 134.48% and more substantial than that of the conventional sensor.

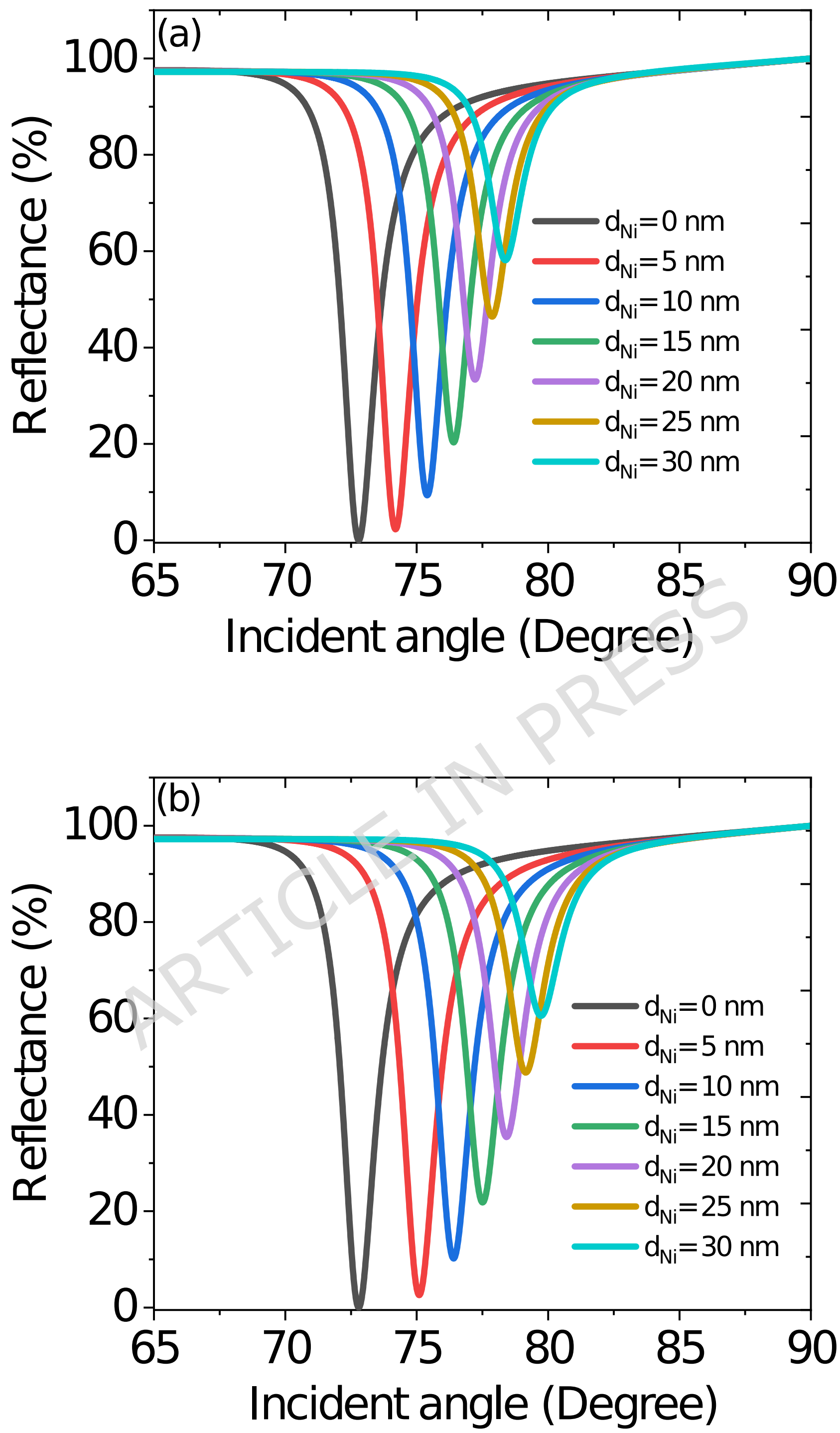

Fig. 4. Reflectance curve for the suggested nanostructure BK7/Ag/BiFeO3/Ni/SM, computed as an incidence angle for varying Ni layer thicknesses; (a) for EC= 0%, (b) for EC= 10%.

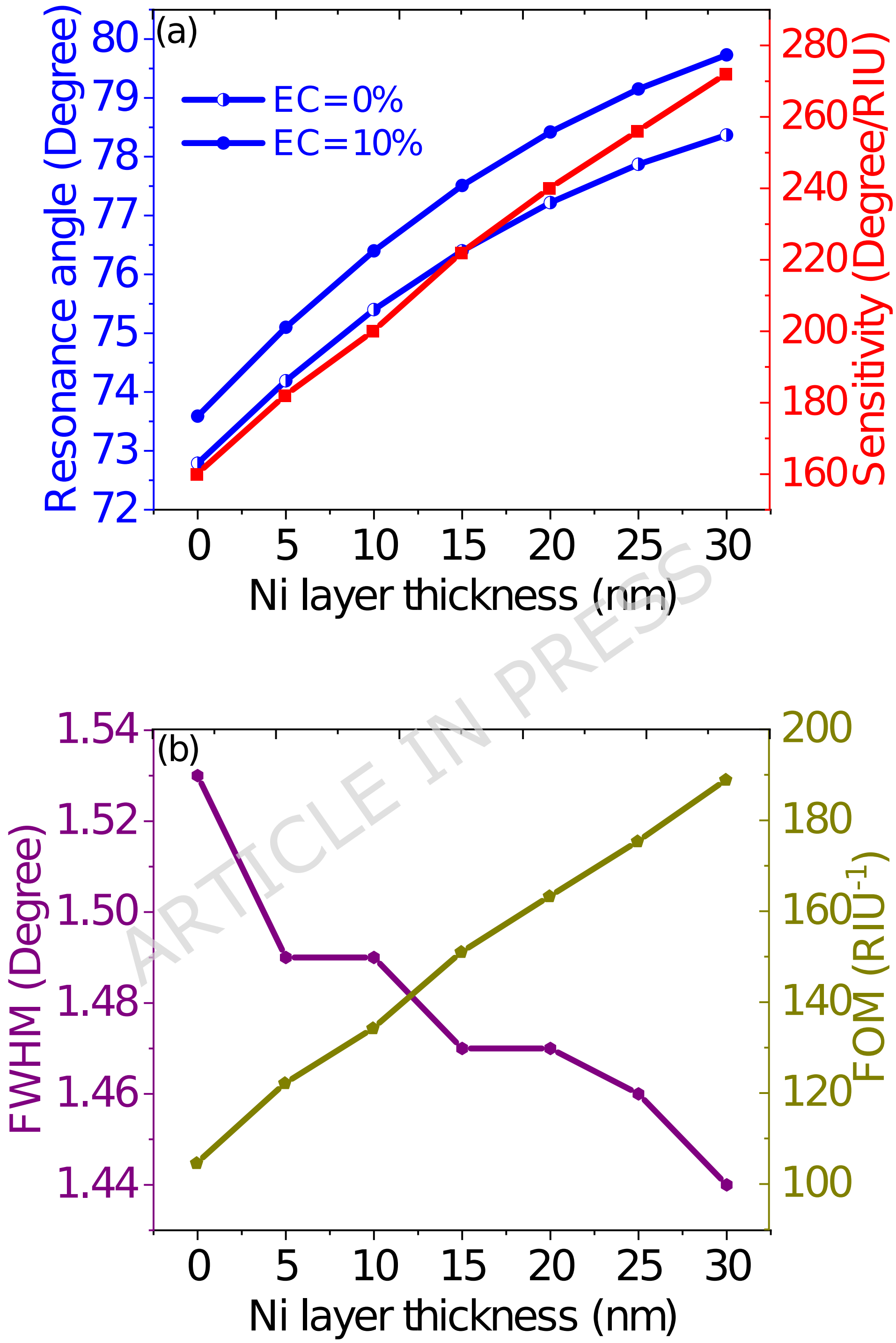
(a)
EC=0%
EC=10%
Resonance angle (Degree)
Sensitivity (Degree/RIU)
80
79
78
77
76
75
74
73
72
280
260
240
220
200
180
160
0
5
10
15
20
25
30
Ni layer thickness (nm)
(b)
FWHM (Degree)
FOM (RIU^{-1})
1.54
1.52
1.50
1.48
1.46
1.44
200
180
160
140
120
100
0
5
10
15
20
25
30
Ni layer thickness (nm)

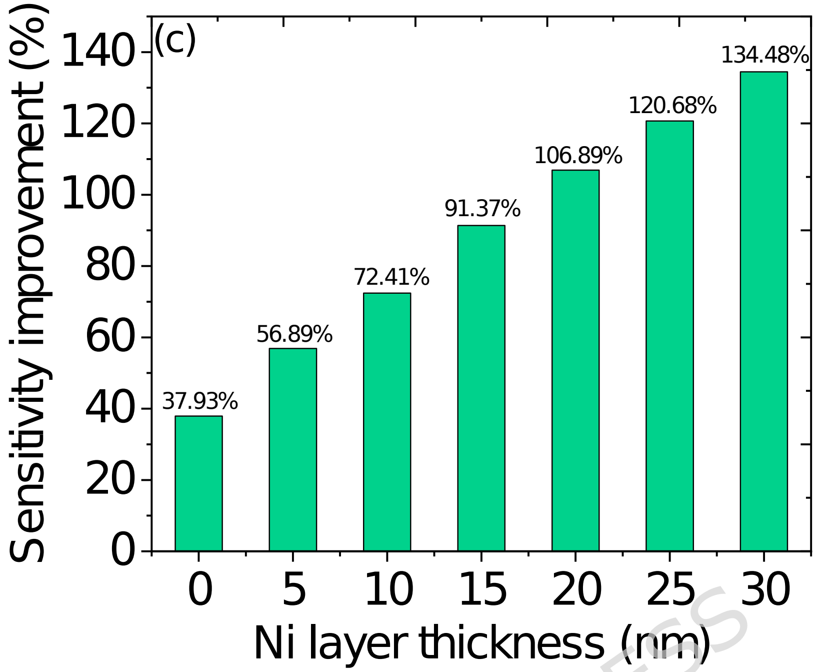

Fig. 5. (a) Sensitivity augmentation vs Ni layer thickness for the suggested biosensor (b) FWHM and FOM variation as a function of Ni layer thickness, and (c) evolution of the resonance angle and angular sensitivity.

Effect of the $MAPbBr_3$ layer

When the RI of the sensing medium is altered from EC= 0% to 10% at dBiFeO3 = 5 nm and dNi = 20 nm, a value of 240 deg/RIU is obtained. As we saw in the previous section, the inclusion of BiFeO3 and Ni sheets rallies the efficiency of the suggested structure. We will now incorporate MAPbBr3, another material from the perovskite family, into the suggested SPR nanostructure in order to observe an improved biosensor design [41–43]. With the optimal thicknesses for the SPR nanostructure (BK7/Ag(55 nm)/BiFeO3(5 nm)/Ni(20 nm)/SM) without the MAPbBr3 film remaining constant, the thickness of the MAPbBr3 sheet is adjusted. We have examined the impact of the MAPbBr3 sheet on the performance parameters with the perovskite thickness (d□□□□□□3) in order to examine how it affects the performance of the suggested SPR biosensor. First, as seen in Figure 6(a) and (b), we examined the impact of a few MAPbBr3 sheets (0 - 3.5 nm) on the reflectivity spectrum while the analyte's EC is amended at EC = 0% and EC = 10%. As d□□□□□□3 rises, both data demonstrate a decline in the resonant dip and its efficiency. Figure 7(a) presents the development of the resonant angle against d□□□□□□3 to demonstrate the benefit of including the MAPbBr3 layer within the nanostructure. As d grows from 0 to 3.5 nm, we get a quasi-linear increase of the SPR angle. The sensitivity variation as a function of d□□□□□□3 is depicted by the red curve in Figure 7(a). When the thickness of d□□□□□□3 = 3 nm, we can see a high sensitivity of 428 deg/RIU, where there is no discernible optical response for $d_{□□□□□□3}$ > 3. Figure. 7(b) displays the development of FOM and FWHM with $d_{□□□□□□3}$. The FWHM rises from 1.47 deg to 3.37 deg when d□□□□□□3 is increased from 0 to 3.5 nm, demonstrating a decline in the SPR biosensor's detection accuracy. Figure 7(b)'s yellow brown curve illustrates how changing d from 0 to 3.5 causes the FOM to drop from 163.26 RIU−1 to 149.12 RIU−1. Figure 7(c) illustrates how our researched design outperforms the typical sensor in terms of sensitivity compared to d□□□□□□3. Observe that the SPR biosensor suggested in this paper has a significant increase in sensitivity of 268.96%. This is the ideal value for d□□□□□□3 = 3 nm. The perovskite sheet of MAPbBr3 is found to be crucial in enhancing the SPR biosensor's detection capabilities.

In order to obtain acceptable resonance and great sensitivity, the sensing medium's range of ethanol concentrations is a crucial design parameter for the SPR sensor. We were able to identify the proper EC variation scope for a sensitive sensor by examining the effects of various EC of the sensing medium [44,45]. The development of resonant dip with the sensing medium's EC is depicted in Figure 8. We utilized the best values found in the preceding sections for the remaining parameters (d□□□□□3 = 5 nm, d□□ = 20 nm, and d□□□□□□3 = 3 nm).

The SPR resonance angle fluctuation with EC is displayed in Figure 8(a). The four SPR nanostructures' sensitivity changes with ethanol concentration (EC) are depicted in Fig. 8(b). With the exception of the Ag/BiFeO3/Ni/MAPbBr3 design, where the sensitivity decreases for EC > 20%, the sensitivity of the four designs under study only increases for EC between 10% and 40%. The MAPbBr3 perovskite layer allows the suggested biosensor to achieve its maximum sensitivity between EC = 10% and EC = 20%.

Table 2 compares the superior performance achieved by the suggested SPR schemes with various layer combinations of nanomaterials examined in this work, based on the research and analysis mentioned above. We demonstrate that the suggested SPR biosensor based on the perovskite layer may be applied to numerous sensing nanotechnology domains by comparing the tabular performance of our proposed work with that of a standard SPR sensor.

Lastly, to contrast our suggested SPR structure with the most recent SPR structures that have been published by various research teams. Table 3 is where the findings are grouped. Take note of Table 3, which unequivocally demonstrates that our work's efficiency are greater than those of any other finding that has been published in the literature. Consequently, the most efficient sensor for organic and chemical detection is still our SPR sensor.

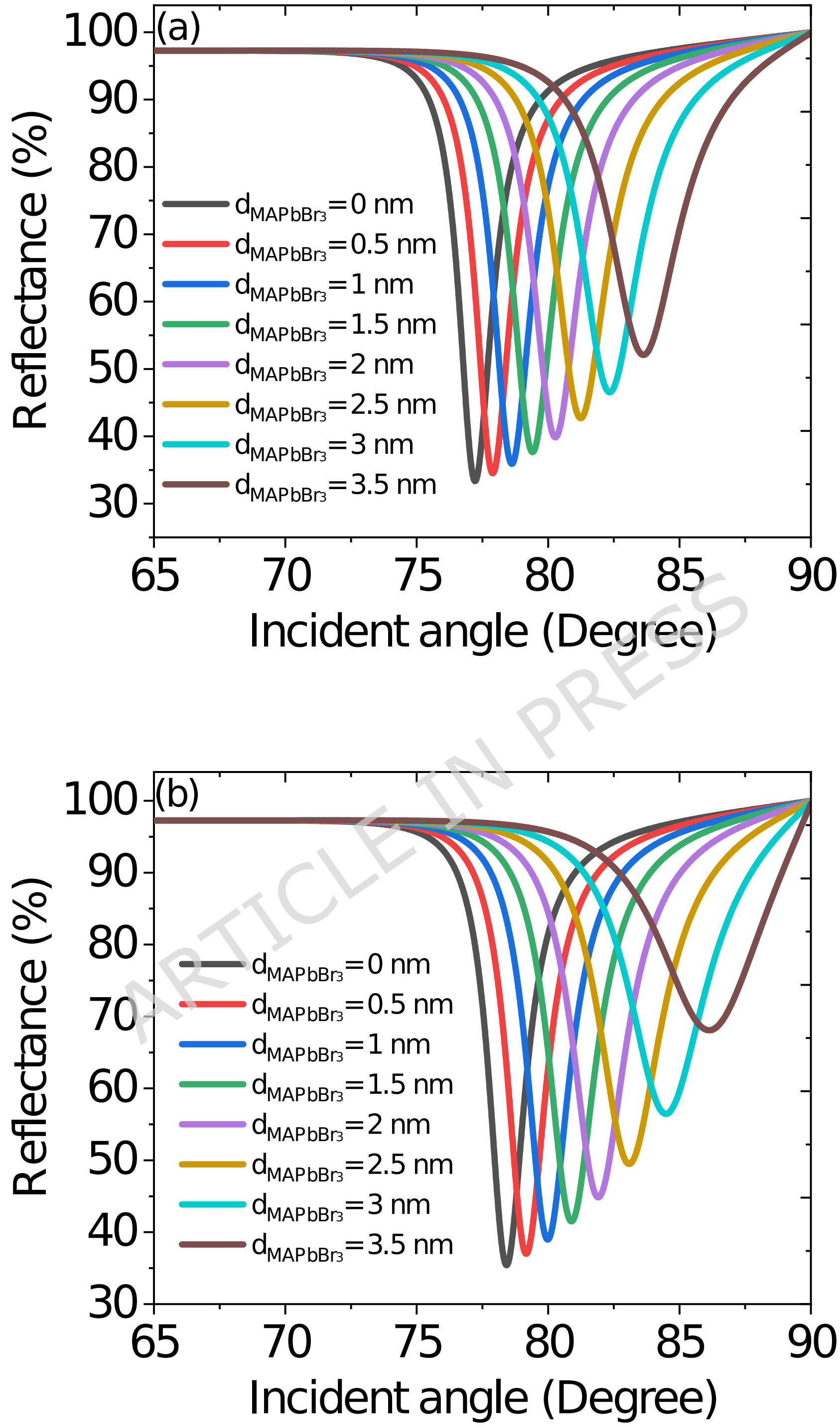

Fig. 6. Reflectance with the perovskite thickness (d_{MAPbBr_3}) in the suggested structure; (a) for EC= 0%, (b) for EC= 10%.

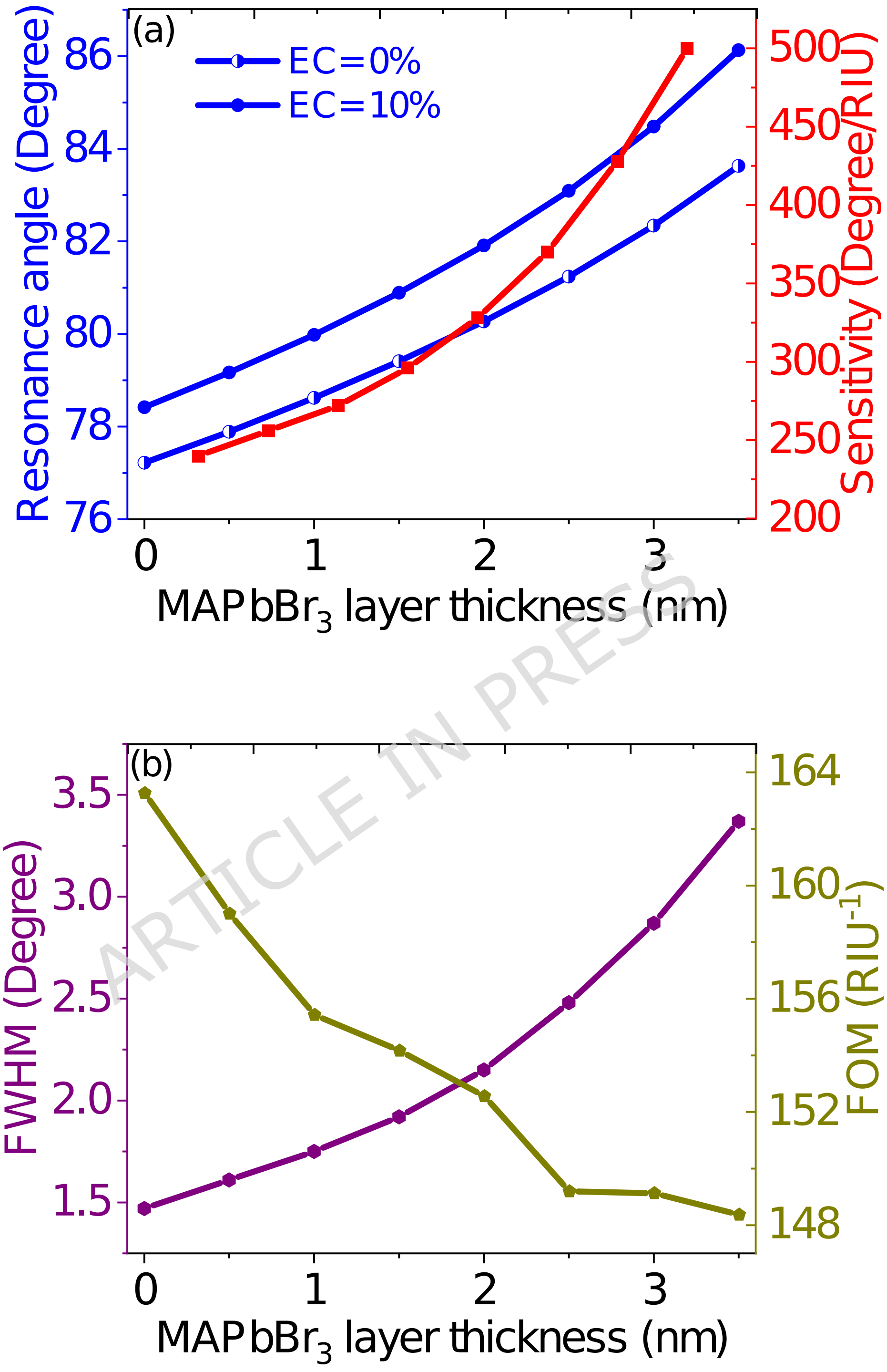

(a)
EC=0%
EC=10%
Resonance angle (Degree)
Sensitivity (Degree/RIU)
76
78
80
82
84
86
200
250
300
350
400
450
500
0
1
2
3
MAPbBr3 layer thickness (nm)
(b)
FWHM (Degree)
FOM (RIU-1)
1.5
2.0
2.5
3.0
3.5
148
152
156
160
164
0
1
2
3
MAPbBr3 layer thickness (nm)

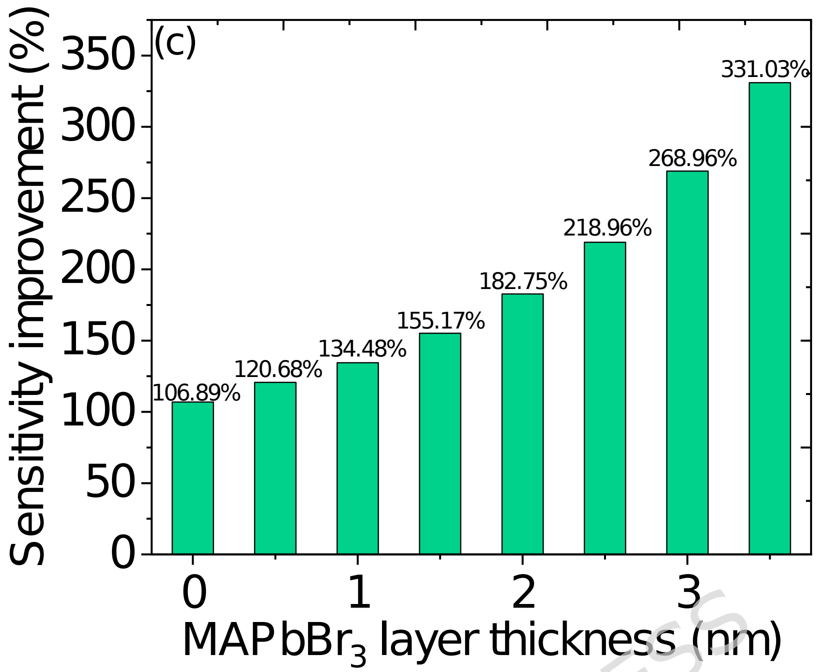

Fig. 7. (a) Sensitivity enhancement fluctuation with perovskite layer thickness (d□□□□□□3) , (b) FWHM and FOM, and (c) resonance angle and sensitivity evolution

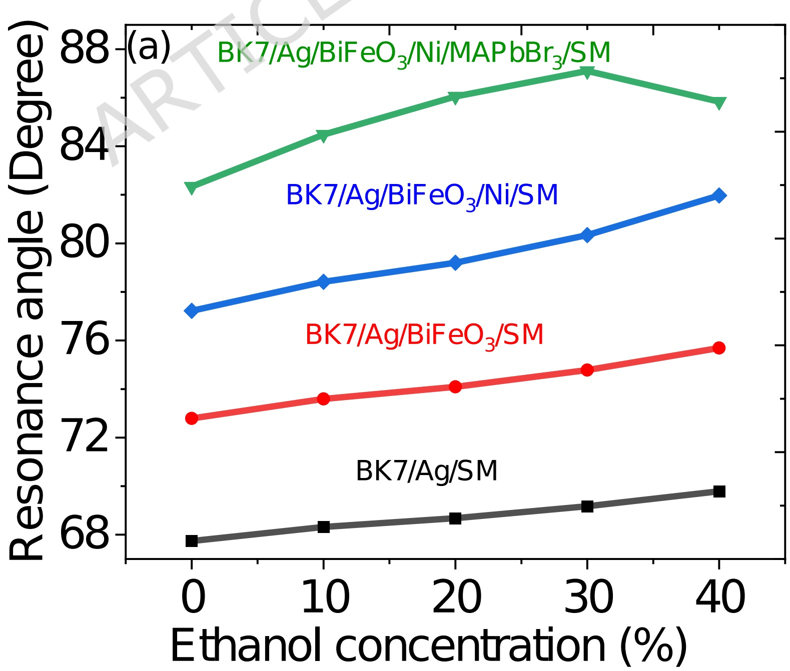

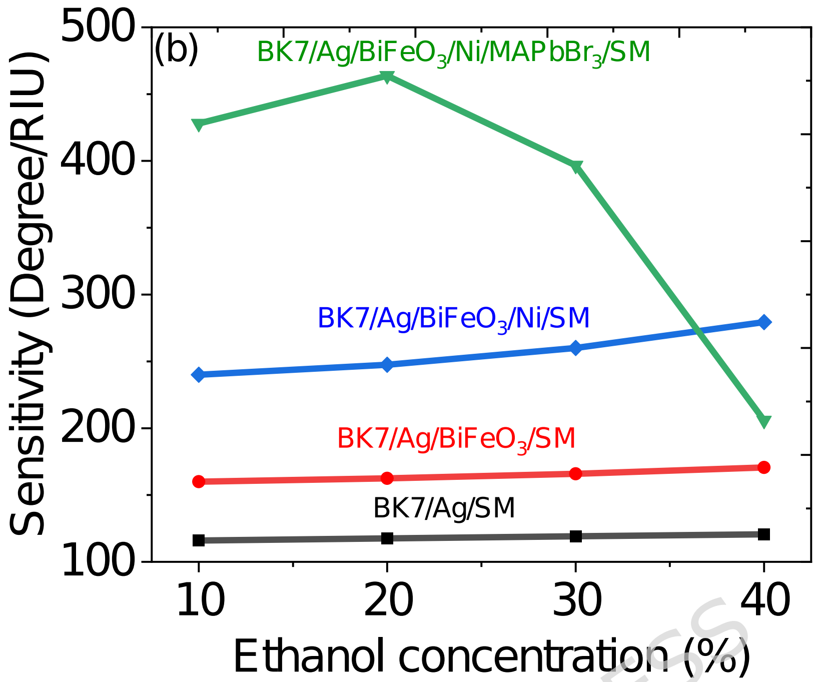

Fig. 8. (a) SPR resonance angle and (b) angular sensitivity versus EC of the sensing medium.

Table 2. Performance characteristics of the suggested SPR schemes for the biosensor are compared.

Proposed SPR designs	θ_{SPR} (Degree) of EC= 0%	R_{min} (%)	Sensitivity (Degree RIU^{-1}) of EC= 10%	FWHM (Degree) of EC= 10%	FOM (RIU^{-1}) of EC= 10%	Sensitivity enhancement (%)
BK7/Ag/SM	67.74	0.0247	116	0.77	150.64	-
BK7/Ag/ $BiFeO_3$/SM	72.79	0.001	160	1.53	104.57	37.93
BK7/Ag/ $BiFeO_3$/Ni/ SM	77.22	33.35	240	1.47	163.26	106.89
BK7/Ag/ $BiFeO_3$/Ni/ $MAPbBr_3$ /SM	82.34	46.55	428	2.87	149.12	268.96

Table 3. Comparative analysis of the suggested work at 633 nm wavelength with the majority of recent related work.

Techniques/structures	Sensitivity (Degree RIU^{-1})	FOM (RIU^{-1})	Year	Reference
BK7/Ag/TiO_2/$MAPbX_3$/graphene/SM	255.8	126	2021	[14]
BK7 prism/Cu/Ni/BP/$Ti_3C_2T_{\square}$/SM	304.47	57.85	2021	[13]
BK7/Ag/$BiFeO_3$/graphene/SM	303	43.06	2021	[16]
BK7/Ni/BlueP /SM	270	27.73	2021	[20]
BK7/Ag/BaTiO3/Ag/BP/SM	360	72.6	2022	[46]
CaF_2/Ag/Fe_2O_3/Ni/BlueP-$MoSe_2$/SM	395	90	2022	[12]
BK7/Ag/Si/Ag/WSe_2/SM	373	-	2024	[47]
BK7/Ni/Al_2O_3/BlueP-WSe_2/SM	298.55	-	2025	[48]
BK7/Ag/TiO2/Ni/ BP /SM	299.42	-	2025	[49]
BK7/Ag/$BiFeO_3$/Ni/$MAPbBr_3$/SM	428	149.12	Current work	Current work

Conclusion

In this work, an SPR biosensor aided by the BK7/Ag/BiFeO3/Ni/MAPbBr3/SM structure detects ethanol at a wavelength of 633 nm. The transfer matrix approach is used to analyze the sensor's performance in terms of resonance angle, minimum reflectance, FWHM, sensitivity, and FOM. In order to achieve optimal performance, the thickness of the BiFeO3, Ni, and MAPbBr3 layers was adjusted, while the silver (Ag) layer was fixed at 55 nm. According to the analyzed results, for a 10% EC variation between EC = 0% and 10%, the suggested sensor with the perovskite sheet (MAPbBr3) achieves a very high sensitivity of 428 Degree RIU-1 with a matching FOM of 149.12 RIU-1. Comparing the suggested sensor construction to the traditional configuration (BK7/Ag/SM), a notable sensitivity improvement of 268.96% is demonstrated. Four distinct sensor structures: conventional (BK7/Ag/SM), with BiFeO3 (BK7/Ag/BiFeO3/SM), with Ni (BK7/Ag/BiFeO3/ Ni/SM), and our suggested sensor structure (BK7/Ag/BiFeO3/Ni/ MAPbBr3/ SM) were examined and their performances compared.

Author contribution statement

Malek G. Daher: Conceptualization**,** writing original draft; **Malek G. Daher:** Design, editing original draft and formal analysis **Samer M. Srour:** Simulation, creating figures and graph; **Samer M. Srour:** formal analysis; **Supervision, Funding, reviewing and edition:** Emad Solouma, Stefano Bellucci, Haifa A. Alqhtani, Hussein A. Elsayed, and Ahmed Mehaney and Mostafa R. Abukhadra.

Funding: The authors acknowledge Princess Nourah bint Abdulrahman University Researchers Supporting Project number (PNURSP2025R458), Princess Nourah bint Abdulrahman University, Riyadh, Saudi Arabia.

Acknowledgment: The authors acknowledge Princess Nourah bint Abdulrahman University Researchers Supporting Project number (PNURSP2025R458), Princess Nourah bint Abdulrahman University, Riyadh, Saudi Arabia.

Availability of Data and Material: Simulation software.
Data Availability: The datasets generated and analyzed during the current study are available from the corresponding author on reasonable request**.**
Declarations
Ethics Approval: Not applicable.
Consent to Participate: Not applicable.
Consent for Publication: Not applicable.
Conflict of interest: No competing interests

References

[1] S. Singh, P.K. Singh, A. Umar, P. Lohia, H. Albargi, L. Castañeda, D.K. Dwivedi, 2D nanomaterial-based surface plasmon resonance sensors for biosensing applications, Micromachines 11 (8) (2020) 779.

[2] Raikwar, S., Srivastava, D.K., Saini, J.P. *et al.* 2D-antimonene-based surface plasmon resonance sensor for improvement of sensitivity. *Appl. Phys. A* **127**, 92 (2021). https://doi.org/10.1007/s00339-020-04248-0.

[3] Alhawari, A.R.H., Almawgani, A.H.M., Daher, M.G. *et al.* A Novel Surface Plasmon Resonance (SPR) Sensor Based on Beryllium Oxide and Graphene Layers for Fuel Adulteration Discovery. *Plasmonics* **20**, 5363–5372 (2025). https://doi.org/10.1007/s11468-024-02657-y.

[4] H. Vaisocherova, J. Homola, SPR biosensors for medical diagnostics, in: Surface Plasmon Resonance Based Sensors, Springer, Berlin, Heidelberg, 2006, pp. 229–247.

[5] M. El Barghouti, A. Akjouj, A. Mir, High-performance bimetallic layer plasmonic sensors: a comparative study among Ti_3C_2T▯ black phosphorus and WS2, Appl. Phys. A 128 (3) (2022) 1–15.

[6] Adam, Y.S., Almawgani, A.H.M., Daher, M.G. *et al.* Novel Polymer-based Surface Plasmon Resonance Nanostructure for the Rapid Detection of

Glucose and BSA Concentrations. *Plasmonics* **20**, 4425–4438 (2025). https://doi.org/10.1007/s11468-024-02628-3.

[7] Daher, M.G., Taya, S.A., Faragallah, O.S. *et al.* Detection of protozoa in drinking water using SPR biosensor employing titanium dioxide and MXene nanomaterial. *J Comput Electron* **24**, 45 (2025). https://doi.org/10.1007/s10825-025-02280-y

[8] Raikwar, S., Prajapati, Y.K., Srivastava, D.K. *et al.* Detection of Leptospirosis Bacteria in Rodent Urine by Surface Plasmon Resonance Sensor Using Graphene. *Photonic Sens* **11**, 305–313 (2021). https://doi.org/10.1007/s13320-020-0587-2

[9] Y. Liu, N.O. Weiss, X. Duan, H.C. Cheng, Y. Huang, X. Duan, Van der waals heterostructures and devices, Nat. Rev. Mater. 1 (2016) 16042.

[10] M. El barghouti, O. Haidar, A. Akjouj, A. Mir, Figure of merit and sensitivity enhancement of biosensor LSPR in investigated for visible and near infrared, Photon. Nanostruct. Fundam. Appl. (2022) 101016.

[11] J. Homola, S.S. Yee, G. Gauglitz, Surface plasmon resonance sensors: review, Sensors Actuators B 54 (1999) 3–15.

[12] S. Singh, A.K. Sharma, P. Lohia, D.K. Dwivedi, Ferric oxide and heterostructure BlueP/MoSe2 nanostructure based SPR sensor using magnetic material nickel for sensitivity enhancements, Superlattices Microstruct. (2021) 107126.

[13] R. Kumar, S. Pal, N. Pal, V. Mishra, Y.K. Prajapati, High-performance bimetallic surface plasmon resonance biochemical sensor using a black phosphorus-MXene hybrid structure, Appl. Phys. A 127 (4) (2021) 1–12.

[14] J. Hakami, A. Abassi, A. Dhibi, Performance enhancement of surface plasmon resonance sensor based on Ag-TiO_2-$MAPbX_3$-graphene for the detection of glucose in water, Opt. Quantum Electron. 53 (4) (2021) 1–17.

[15] M. El Barghouti, A. Akjouj, A. Mir, Enhancement of localized surface plasmon resonances of silver nanoparticles array upon the presence of graphene coatings: LSPR biosensor, IOP Conf. Series: Mater. Sci. Eng. 783 (2020) 012023.

[16] C. Li, Z. Li, S. Guo, X. Li, Q. Cheng, S. Meng, Sensitivity enhancement by employing BiFeO3 and graphene hybrid structure in surface plasmon resonance biosensors, Opt. Mater. 121 (2021) 111618.

[17] A. Paliwal, A. Sharma, M. Tomar, V. Gupta, Magneto-optical properties of BiFeO3 thin films using surface plasmon resonance technique, Physica B 448 (2014) 120–124.

[18] D. Sando, C. Carrétéro, M.N. Grisolia, A. Barthélémy, V. Nagarajan, M. Bibes, Revisiting the optical band gap in epitaxial BiFeO3 thin films, Adv. Opt. Mater.6 (2) (2018) 1700836.

[19] G. AlaguVibisha, J.K. Nayak, P. Maheswari, N. Priyadharsini, A. Nisha, Z. Jaroszewicz, R. Jha, Sensitivity enhancement of surface plasmon resonance sensor using hybrid configuration of 2D materials over bimetallic layer of Cu–Ni, Opt. Commun. 463 (2020) 125337.

[20] N. Liu, S. Wang, Q. Cheng, B. Pang, J. Lv, High sensitivity in Ni-based SPR sensor of blue phosphorene/transition metal dichalcogenides hybrid nanostructure, Plasmonics 16 (5) (2021) 1567–1576.

[21] Z.T. Huang, C.W. Yin, Y.H. Hong, H. Li, K.B. Hong, T.S. Kao, T.C. Lu, Hybrid plasmonic surface lattice resonance perovskite lasers on silver nanoparticle arrays, Adv. Opti. Mater. 9 (17) (2021) 2100299.

[22] J. Kim, H. Son, D.J. Cho, B. Geng, W. Regan, S. Shi, K. Kim, A. Zett, Y.A. Shen, F. Wang, Electrical control of optical plasmon resonance with graphene, Nano. Lett. 12 (2012) 5598–5602.

[23] A. Kojima, K. Teshima, Y. Shirai, T. Miyasaka, Organometal halide perovskites as Visible-light sensitizers for photovoltaic cells, J. Am. Chem. Soc. 131 (2009) 6050–6051.

[24] H. S. Gumaih, A. H. M. Almawgani, M. G. Daher, Y. S. Adam, S. A. Taya, and Y. K. Prajapati, “Theoretical Optimization of Silver-Based Surface Plasmon Resonance Sensor with Perovskite and Graphene Composite Structure for the Rapid Detection of Breast Cancer Cells,” Plasmonics, 2025, doi: 10.1007/s11468-024-02753-z.

[25] M. G. Daher, Y. Trabelsi, N. M. Ahmed, Y. K. Prajapati, A. N. Z. Rashed, and S. K. Patel, "Detection of Escherichia coli using highly sensitive surface plasmon resonance nanostructure (SPRN) based on MXene 2D nanomaterial," Plasmonics, vol. 18, no. 6, pp. 2483-2492, 2023.

[26] P. Sun, M. Wang, L. Liu, et al., “Sensitivity enhancement of surface plasmon resonance biosensor based on graphene and barium titanate layers,” Appl. Surf. Sci. 475, 342–347 (2019).

[27] G. Kumar, J. Schroers, Write and erase mechanisms for bulk metallic glass, Appl. Phys. Lett. 92 (3) (2008) 031901.

[28] Y. Vasimalla, H.S. Pradhan, A highly performed SPR biosensor based on bismuth ferrite-bromide materials-BP/graphene hybrid structure, Opt. Quantum Electron. 53 (12) (2021) 1–18.

[29] B. Karki, S. Sharma, Y. Singh, A. Pal, Sensitivity enhancement of surface plasmon resonance biosensor with 2-D franckeite nanosheets, Plasmonics 17 (1) (2022) 71–78.

[30] Y. Li, J. Gao, X. Lu, An effective antioxidized strategy for Ag based film-dierlectricmetal plasmonic sensor, NUSOD IEEE (2016) 73–74.

[31] H. Mohamed Ilyes, D. Oualid, H. Ghania, and M. Aissa, "Enhanced Surface Plasmon Resonance Biosensor Using Silver, Perovskite Oxides, and MXene Nanostructures for Sensitive Blood Cancer Detection," Plasmonics, Jun. 2025, doi: 10.1007/s11468-025-03071-8.

[32] V. Sharma, A. Kumar, S. Saharan, and S Semwal, Graphene/Au/MIP-Coated D-Shaped Optical Fiber–Based SPR Sensor for Ethanol Detection, Plasmonics 18, (2023) 1639–1649.

[33] A. M. Pillai, N. Nair, M. K. Das, and S. K. Ram, "Strategic approaches to enhance efficiency and commercial feasibility of copper-based surface plasmon resonance sensing," Next Materials, vol. 7, Apr. 2025, doi: 10.1016/j.nxmate.2024.100377.

[34] R. Slavík, J. Homola, and H. Vaisocherová, "Advanced biosensing using simultaneous excitation of short and long range surface plasmons," Meas Sci Technol, vol. 17, no. 4, pp. 932–938, Apr. 2006, doi: 10.1088/0957-0233/17/4/045.

[35] S. Roy et al., "Numerical investigation into impact of halide perovskite material on the optical performance of prism-loaded hybrid surface plasmon resonance biosensor: A strategy to increase sensitivity," Sens Biosensing Res, vol. 43, 2024, doi: 10.1016/j.sbsr.2024.100630.

[36] M. Mishra, S. Senapati, A. Yadav, and S. K. Tripathy, "BaTiO3 boosted silver-based SPR sensor for efficient urine-glucose detection in pre-diabetic and early-diabetic stages," Sens Actuators A Phys, vol. 379, Dec. 2024, doi: 10.1016/j.sna.2024.115895.

[37] M. N. Sakib et al., "High performance dual core D-shape PCF-SPR sensor modeling employing gold coat," Results Phys, vol. 15, Dec. 2019, doi: 10.1016/j.rinp.2019.102788.

[38] H. Kushwah and J. K. Anand, "Enhanced detection accuracy and signal-to-noise ratio of surface plasmon resonance based refractive index sensor with the addition of thicker layer of Silicon," Opt Mater (Amst), vol. 140, p. 113862, Jun. 2023, doi: 10.1016/j.optmat.2023.113862.

[39] R. Kumar, S. Pal, N. Pal, A. Verma, J.P. Saini, Y.K. Prajapati, Figure of merit enhancement of Ti_3C_2T□-graphene based long-range surface plasmon sensor at telecommunication wavelength, Opt. Quantum Electron. 53 (2021) 1–15.

[40] A. Nisha, P. Maheswari, P.M. Anbarasan, K.B. Rajesh, Z. Jaroszewicz, Sensitivity enhancement of surface plasmon resonance sensor with 2D material covered noble and magnetic material (Ni), Opt. Quantum Electron. 51 (2019) 1–12.

[41] L. Wu, Y. Xiang, Y. Qin, CH3NH3PbBr3 thin film served as guided-wave layer for enhancing the angular sensitivity of plasmon biosensor, Biosensors 11 (2021) 415.

[42] H. Peng, J. Guo, G. Chen, W. Qin, Self-powered perovskite CH3NH3PbBr3 field effect transistor with fast response and high sensitivity in sensing, Mater. Today Adv. 12 (2021) 100185.

[43] R. Chen, K. Zhan, Y. Wu, Y. Zhu, J. Yan, B. Liu, Y. Chen, A novel fluorescence probe based MAPbBr3@ZIF-8 for detecting hypochlorite in water samples, Microchem. J. 172 (2022) 106924.

[44] M.K. Singh, V.K. Verma, S. Pal, Y.K. Prajapati, J.P. Saini, Antimonene mediated long-range SPR imaging sensor with ultrahigh imaging sensitivity and figure of merit, Opt. Mater. 121 (2021) 111484.

[45] S.E. Zaki, A. Mehaney, H.M. Hassanein, A.H. Aly, High-performance liquid sensor based one-dimensional phononic crystal with demultiplexing capability, Mater. Today Commun. 26 (2021) 102045.

[46] B. Karki, A. Pal, Y. Singh, S. Sharma, Sensitivity enhancement of surface plasmon resonance sensor using 2D material barium titanate and black phosphorus over the bimetallic layer of Au, Ag, and Cu, Opt. Commun. 508 (2022) 127616.

[47] Daher, M.G., Taya, S.A., Faragallah, O.S. *et al.* Optical Detection of Urea Level in Blood Using Novel SPR Sensor Employing Silicon and Tungsten Diselenide Nanomaterial for the Early Diagnosis of Heart and Kidney Diseases. *Plasmonics* **20**, 3853–3862 (2024). https://doi.org/10.1007/s11468-024-02588-8

[48] Daher, M.G., Halim, M.M., Ahmed, N.M. *et al.* An Optical Surface Plasmon Resonance Device (OSPRD) for the Accurate Detection of Injurious Heavy Metals. *Plasmonics* **20**, 8027–8037 (2025). https://doi.org/10.1007/s11468-025-02839-2

[49] Daher, M.G., Taya, S.A., Faragallah, O.S. *et al.* Designing of High-Sensitivity Optical Surface Plasmon Resonance Sensor (OSPRS) for Fast and Accurate Diagnosis of Dengue Virus (DeVs). *Plasmonics* **20**, 3887–3895 (2025). https://doi.org/10.1007/s11468-024-02593-x